ARTICLE

Loss of α-actinin-3 during human evolution provides superior cold resilience and muscle heat generation

Victoria L. Wyckelsma,[1,6] Tomas Venckunas,[2,6] Peter J. Houweling,[3,4] Maja Schlittler,[1] Volker M. Lauschke,[1] Chrystal F. Tiong,[3,4] Harrison D. Wood,[3,4] Niklas Ivarsson,[1] Henrikas Paulauskas,[2] Nerijus Eimantas,[2] Daniel C. Andersson,[1,5] Kathryn N. North,[3,4] Marius Brazaitis,[2,7,*] and Håkan Westerblad[1,2,7,*]

Summary

The protein α-actinin-3 expressed in fast-twitch skeletal muscle fiber is absent in 1.5 billion people worldwide due to homozygosity for a nonsense polymorphism in *ACTN3* (R577X). The prevalence of the 577X allele increased as modern humans moved to colder climates, suggesting a link between α-actinin-3 deficiency and improved cold tolerance. Here, we show that humans lacking α-actinin-3 (XX) are superior in maintaining core body temperature during cold-water immersion due to changes in skeletal muscle thermogenesis. Muscles of XX individuals displayed a shift toward more slow-twitch isoforms of myosin heavy chain (MyHC) and sarcoplasmic reticulum (SR) proteins, accompanied by altered neuronal muscle activation resulting in increased tone rather than overt shivering. Experiments on *Actn3* knockout mice showed no alterations in brown adipose tissue (BAT) properties that could explain the improved cold tolerance in XX individuals. Thus, this study provides a mechanism for the positive selection of the *ACTN3* X-allele in cold climates and supports a key thermogenic role of skeletal muscle during cold exposure in humans.

Introduction

The sarcomeric protein α-actinin-3 resides in the Z-discs of fast-twitch skeletal muscle fibers, where it cross-links the actin filaments of adjacent sarcomeres.[1–3] α-actinin-3 is absent in 1.5 billion people worldwide due to homozygosity for a nonsense polymorphism in *ACTN3* (R577X).[4] The lack of functioning *ACTN3* (MIM: 102574) does not cause muscle disease, but it has been shown to affect muscle function both in the general population and in athletes;[5,6] in general, α-actinin-3 deficiency (MIM: 617749) is detrimental for power and sprint activities.[5,7,8]

A study exploring evolutionary implications of α-actinin-3 deficiency demonstrated that the X-allele became more abundant as humans migrated out of Africa into the colder climates of central and northern Europe.[4,9,10] This led to the hypothesis that α-actinin-3-deficient humans are superior in adapting to lower temperature.[9] On this basis, we sought to determine whether α-actinin-3-deficient (XX) humans were better at defending their body temperature during an acute cold challenge than humans with functioning *ACTN3* (RR).

Material and methods

Participants, mice, and ethical approval

Humans

Healthy young (18–40 years) males were recruited to participate in the study. Before being included in the study, each participant was informed of the aims, the experimental procedures, and the potential risks of the study and signed a written informed consent form consistent with the principles outlined in the Declaration of Helsinki. The study was approved by Kaunas Regional Biomedical Research Ethics Committee (license number BE-2-30). All experiments were performed double-blinded regarding the *ACTN3* genotype.

The participants were residents in a modern town (Kaunas) and hence subjected to a typical city lifestyle. They were moderately physically active (<2 h physical exercise/week) and did not participate in any formal physical exercise or sport program. They did not have occupations where they were exposed to prolonged cold challenges and they had not been involved in any temperature manipulation program or extreme-temperature exposure (e.g., ice water bath after physical exercise or swimming in open cold water) for at least 3 months. Individuals with any existing medical condition or taking medication that could affect natural thermoregulation were excluded from the study. The physical characteristics of the participants are presented in Table S1. Their weight (in kg), body fat percentage (TBF-300 body composition analyzer, Tanita, UK),

[1]Department of Physiology and Pharmacology, Biomedicum, Karolinska Institutet, 171 77 Stockholm, Sweden; [2]Institute of Sport Science and Innovations, Lithuanian Sports University, 44221 Kaunas, Lithuania; [3]Murdoch Children's Research Institute, The Royal Children's Hospital Melbourne, Melbourne, VIC 3052, Australia; [4]Department of Paediatrics, Melbourne Medical School, University of Melbourne, Melbourne, VIC 3010, Australia; [5]Heart, Vascular and Neurology Theme, Cardiology unit, Karolinska University Hospital, 171 76 Stockholm, Sweden
[6]These authors contributed equally
[7]These authors contributed equally
*Correspondence: marius.brazaitis@lsu.lt (M.B.), hakan.westerblad@ki.se (H.W.)
https://doi.org/10.1016/j.ajhg.2021.01.013.

and height (in cm) were measured, and body mass index was calculated. Body surface area (in m^2) was estimated as previously described using the following formula: body surface area = $128.1 \times \text{Weight}^{0.44} \times \text{Height}^{0.60}$.[11] Skinfold thickness (in mm) was measured with a skinfold calliper (SH5020, Saehan) at ten sites (chin, subscapular, chest, side, suprailium, abdomen, triceps, thigh, knee, and calf) and the mean subcutaneous fat layer thickness was calculated.[12]

Actn3 *KO and WT mice*

All animal work was carried out in accordance with approval from the Murdoch Children's Research Institute Animal Care and Ethics Committee (Approval No. A760). Animals were housed in a specific-pathogen-free environment at a constant ambient temperature of 22°C and 50% humidity on a 12 h light-dark cycle, with *ad libitum* access to food and water, unless otherwise specified. Generation of *Actn3* KO mice on a C57BL/6J background has been previously reported.[13] Age-matched 3-month-old female WT and *Actn3* KO littermates derived from heterozygous *Actn3* crosses were used for all animal studies.

Genotyping

Human

DNA was extracted from blood samples using the NucleoSpin Blood kit (Macherey-Nagel) according to the manufacturer's protocol. *ACTN3* R577X genotype was determined using a PCR-RFLP method as previously described.[14]

Mouse

Actn3 WT and KO genotypes were determined using PCR-RFLP using DNA extracted from ear punch biopsies and extracted as outlined previously.[4]

Acute cold exposure

Human cold-water immersion protocol

An intermittent whole-body water immersion cooling protocol was used as previously described.[15–17] Experiments were conducted indoors at the same time of day (from 7:00 a.m. to 11:00 a.m.). The participants refrained from consuming any food for at least 12 h before the experiment. To standardize the state of hydration and the sensation of thirst, subjects were allowed to drink still water as desired until 60 min before the water immersion session. The experiments were performed at a room temperature of 22°C and a relative humidity of 60%. Prior to cold-water immersion, the participants rested for 10–15 min dressed in a T-shirt, swim shorts, and socks and baseline ventilation parameters, heart rate, and temperatures were measured during the subsequent 20 min. Thereafter, they entered a 14°C water bath with only the head above the surface. Individuals stepped out of the bath every 20 min and rested for 10 min at room temperature, and then returned to the water bath for the next 20 min of cold-water immersion. This intermittent whole-body water immersion procedure continued until either the rectal temperature (T_{re}) had decreased to 35.5°C or a maximum of 120 min of cold-water immersion (170 min including the breaks).

Mouse acute thermoneutral and cold exposure

For acute temperature exposure experiments, 12-week-old female WT and *Actn3* KO mice were singly housed in cages kept at either 30°C or 4°C as previously published.[18] Briefly, mice housed at thermoneutrality (30°C) were acclimatized at this temperature for 20 h (with food and water *ad libitum*) prior to commencement of experiments. Food, water, and bedding were removed from cold-exposed mice during the 5 h cold exposure period.

Body temperature measurements

Humans

T_{re} was measured throughout the experiment using a thermocouple (Rectal Probe, Ellab; accuracy ± 0.1°C) which was inserted by the subjects to a depth of 12 cm past the anal sphincter. Muscle (T_{mu}) and skin (T_{sk}) temperatures were measured before and at the end of the water immersion session. The T_{mu} was measured with a needle microprobe (MKA, Ellab; accuracy ± 0.01°C) inserted ~3.5 cm under the skin covering the lateral gastrocnemius muscle of the right leg. The skin was prepared before each intramuscular temperature measurement by shaving and disinfecting with a cotton-wool tampon soaked with medicinal alcohol. The insertion area was marked to ensure the repeatability of the measurement. T_{sk} was measured with thermistors taped to the back, the thigh, and the forearm (DM852, Ellab; accuracy ± 0.1°C), and mean T_{sk} was calculated as: $T_{sk} = 0.5T_{back} + 0.36T_{thigh} + 0.14T_{forearm}$.[19]

Mice

Core body temperature was measured by a rectal probe (BAT-12 microprobe thermometer) over a 5-h period between the times of 8:00 and 14:00. Temperatures were measured at 0, 30, 60, 90, 120, 180, 240, and 300 min. Body weights were recorded before and after the 5-h temperature measurement period. At the conclusion of the temperature assessment, all mice were euthanized by cervical dislocation and tissues were collected for further analysis.

Human functional measurements

Spirometry and heart rate measurement

A mobile spirometry system (Oxycon Mobile, Jaeger/VIASYS Healthcare) was used to measure VO_2 and VCO_2 on a breath-by-breath basis. Automatic calibration of the gas analyzer and delay time were performed before measurements as described by the manufacturer, i.e., a calibration gas at 180 kPa (15.2% O_2, 5.02% CO_2, and 79.62% N_2) was supplied to attain gain, offset, and delay times within 1%. Heart rate was measured throughout the experiment with a heart rate monitor (S-625X, Polar Electro).

EMG measurement of thermoregulatory muscle activation

Heat-generating muscle activation is pronounced in the chest region and we therefore measured EMG signals in the *pectoralis major* muscle during cold-water immersion.[20,21] After careful preparation of the skin (shaving, abrading, and cleaning with alcohol wipes) to obtain a low impedance (<10 kOhm), a surface EMG sensor (SX230W, Biometrics Co.) with integrated bipolar Ag-AgCl electrodes (10 mm diameter, 20 mm center-to-center distance) and differential amplifier (gain 1000, input impedance 100 MΩ, an input noise < 5 μV, common mode rejection ratio higher than 96 dB) was placed on the right pectoralis major muscle. The ground electrode (R206, Biometrics Co.) was positioned on the wrist of the right hand. The EMG sensor and ground electrode were connected to a portable data acquisition unit (DataLog P3X8, Biometrics Co.) Before measurements, the channel sensitivity was set to 3 V and the excitation output to 4,600 mV as recommended by the manufacturer. EMG signals were digitized and files were stored on a computer for subsequent analyses of the mean frequency (MnF, in Hz) and root mean square (RMS, in mV) using a dedicated software (Biometrics DataLOG) and manual analysis of the rate of burst activity.

Human protein analyses

Muscle biopsies

Prior to cold-water immersion, biopsies from the *vastus lateralis* muscle were collected from a subgroup of RR (n = 11) and XX (n

= 8) individuals. The biopsy site was cleaned with alcohol and anesthetized locally. After making a small skin cut with a scalpel tip, a biopsy needle was inserted perpendicular to the muscle fibers and biopsies were collected with an automatic biopsy device (Bard Biopsy Instrument, Bard Radiology). After collection, muscle biopsies were snap frozen in liquid nitrogen and stored at −80°C until analysis. The skin cut was cleaned and closed with wound closure strips. Biopsies were not collected after cold exposure.

Whole-muscle homogenate preparation

Whole-muscle homogenate was prepared from frozen muscle biopsies for western blots, analysis of MyHC isoform composition, and immunoprecipitation (IP) experiments. Approximately 15 mg of frozen muscle was weighed and homogenized on ice (1:20 w/v) in HEPES lysis buffer (20 mM HEPES, 150 mM NaCl, 5 mM EDTA, 25 mM KF, 5% glycerol, 1 mM Na_3VO_4, 0.5% Triton [pH 7.6]) with Protease Inhibitor (#11836145001, Roche, 1 tablet per 50 mL). After this stage, 70 μL was diluted to 33 μg wet weight muscle μL^{-1} using 3× SDS denaturing solution (0.125 M Tris-HCl, 10% glycerol, 4% SDS, 4 M urea, 10% 2-mercaptoethanol, and 0.001% Bromophenol Blue [pH 6.8]). Finally, samples were further diluted to 2.5 μg wet weight muscle μL^{-1} with 1× SDS solution (3× SDS denaturing solution diluted 2:1 with 1× Tris-HCl [pH 6.8]). A small amount of undiluted homogenate was taken from each RR participant to make a calibration curve included on every gel for western blotting. The remaining undiluted homogenate was used for IP.

Single-fiber collection, fiber-typing, and pooling

Approximately 10 mg of muscle was freeze-dried for 24 h. Biopsies were left in a desiccator in drying pearls (Sigma) at room temperature for 60 min and then placed in −20°C for long-term storage. Between 40 and 60 segments of single fibers were collected from each muscle biopsy and placed in 12 μL of 1× SDS denaturing solution, once collected fibers were kept at room temperature for 60 min and then stored in −80°C until dot blotting.

Each single-fiber segment was fiber-typed using the dot-blotting method as previously described.[22] Briefly, a polyvinyldifluorid (PVDF) membrane was activated in 96% ethanol for 120 s and then activated in transfer buffer containing 20% methanol for 120 s. Following activation, 1 μL from each single fiber tube was spotted on to a membrane. Once the membrane had dried, membranes were reactivated in ethanol (120 s) and transfer buffer (120 s), membranes were washed in ×1 Tris-buffered saline-Tween (TSBT) and then blocked for ∼10 min in 5% blocking buffer (Bio-Rad) in 1× TBST. The membrane was then incubated in primary antibody overnight at 4°C followed by 2 h at room temperature . After washing and incubation with a secondary antibody, membranes were washed with 1× TBST and coated with chemiluminescent substrate (Clarity Max ECL substrate, Bio-Rad) for imaging on Chemidoc MP (Bio-Rad).

In this study, two membranes were prepared simultaneously from each fiber segment. These membranes were probed either for myosin heavy chain (MyHC) II (mouse, monoclonal IgG, A4.74, Developmental Studies Hybridoma Bank [DSHB]) or for MyHC I (mouse, monoclonal IgM, A4.840, DSHB) diluted 1:200 in blocking buffer in PBS (LiCOR Biosciences) 1:1 v/v in 1× TBST. Single-fiber segments of the same fiber type from each muscle biopsy were subsequently pooled into a single tube and frozen at −80°C until western blotting. Each pool ranged between 4 and 15 fibers. Only fiber segments that were identified either as MyHC II or MyHC I were used in subsequent analyses.

Western blotting

Proteins of whole homogenates and pools of single-fiber segments were separated on either 4%–15% TGX stain-free gels or for analysis of sarcolipin (SLN), 16.5% Tris Tricine gels. TGX stain-free gels had total protein visualized prior to transfer and analyzed on Image Lab software (Image Lab 6.0, Bio-Rad).[23] Protein was wet transferred to a PVDF (or nitrocellulose for SLN) membrane for 1 h. Following transfer, tris-tricine gels were stained (Coomassie Brilliant Blue R-250, Bio-Rad) for 2 h at room temperature and de-stained (40% methanol, 10% acetic acid) for 2 × 1 h washes at room temperature and then stored overnight in MilliQ H_2O before being visualized for myosin bands on a Chemi Doc MP (Biorad). Membranes were blocked at room temperature for 2 h using LI-COR blocking buffer with TBS (LI-COR Biosciences). After blocking, membranes were incubated in primary antibody overnight at 4°C and 2 h at room temperature. Primary antibody details are as follows: sarcoplasmic reticulum Ca^{2+}-ATPase (SERCA) 2a (1:5,000, rabbit, A010-20, Badrilla), SERCA1 (1:1,000, mouse, CaF2-5D2, DHSB), calsequestrin (CSQ) 1&2 (1:1,000, mouse, MA3-913, Thermofisher), CSQ2 (1:1,000, rabbit, ab3516, Abcam), ACTN3 (1:1,000, rabbit, ab68204, Abcam), SLN (1:1,000, rabbit, ABT13, Merck Millipore), MyHC II (1:200, mouse IgG,A4.74, DHSB), MyHC I (1:200, Mouse, IgM, A4.840, DSHB), and actin (1:1,000 rabbit, ab1801, Abcam). All antibodies were diluted in LI-COR blocking buffer in PBS (LI-COR Biosciences) 1:1 v/v with 1× TBST. After incubation in primary antibody, membranes were washed in 1× TBST, incubated in secondary antibody (1:20,000, IRDye 680-conjugated donkey anti-mouse IgG and IRDye 800-conjugated donkey anti-rabbit IgG [926–68,072, 926–32,213], LI-COR Biosciences) and immunoreactive bands were visualized using infrared fluorescence (IR-Odyssey scanner, LI-COR Biosciences). Band density was analyzed using Image Studio Lite v 5.2 (LI-COR Biosciences). During data analysis, the density of each sample for a given protein was expressed relative to the calibration curve and then normalized to the total protein of each respective lane. SLN in homogenate was normalized against actin, which was not different between RR and XX individuals. Single-fiber SLN was normalized against Coomassie stain. The same calibration curve was used across all gels and data are expressed relative to the average of the RR subjects on each gel, which was set to 1.0.

Myosin heavy chain composition

MyHC composition was determined by electrophoresis using a protocol adapted from Mizunoya et al.[24] The whole-muscle homogenates were diluted 2.5 times in MilliQ H_2O and then in 2× sample buffer containing 100 mM DTT, 4% w/v SDS, 0.16 M Tris-HCl (pH 6.8), 43% v/v glycerol, and 0.2% bromophenol blue. 100 ng of protein was loaded on a separating gel consisting of 100 mM glycine, 35% v/v glycerol, 200 mM Tris-HCl (pH 8.8), 0.35% w/v SDS, 8.5% w/v acrylamide-*N,N′*-methlyenebisacrylamide (99:1), 0.1% w/v ammonium persulfate, and 0.05% v/v *N,N,N′,N′*-tetramethylethylenediamine. The stacking gel consisted of 10% v/v glycerol, 70 mM Tris-HCl (pH 6.8), 4 mM EDTA, 0.34% w/v SDS, 4% w/v acrylamide-*N,N′*-methlyenebisacrylamide (99:1), 0.1% w/v ammonium persulfate, and 0.05% v/v *N,N,N′,N′*-tetramethylethylenediamine. After adding lower (0.05 M Tris Base, 75 mM glycine, 0.05% w/v SDS) and upper running buffer (6× concentrated lower running buffer with 0.12% v/v 2-mercaptoethanol), electrophoresis was run at 4°C for 40 min at 10 mA and then for 22 h and 20 min at 140 V. After electrophoresis, gels were stained with the SilverXpress Silver Staining Kit (Invitrogen) according to the manufacturer's instruction. Bands were analyzed using ImageJ software.

Immunoprecipitation

For IP, 1 μg anti- ryanodine receptor 1 (RyR1; ab2868, Abcam) antibody was bound to 12 μL G-protein Dynal magnetic beads (10007D, Life Technologies) following the manufacturer's instructions. The lysates were centrifuged at 700 × *g* and 4°C for 10 min

and the protein concentration of the supernatant was determined with the Bio-Rad Protein Assay (#500-0006). The samples were then diluted to 0.5 μg protein per μL and 400 μL of each sample was added to the antibody-bead complex. Samples were incubated overnight at 4°C under gentle rotation. After incubation, samples gently washed four times with HEPES buffer. Samples were placed on a magnet rack for removal of buffer. To remove separate peptides from the beads, 50 μL Laemmli buffer (Bio-Rad) with 5% 2-mercaptoethanol were added and samples were heated for 5 min at 95°C. To remove the beads from the solution, tubes were placed on a magnet and the solution was transferred to fresh tubes. Samples (10 μg/well) were loaded on precast 4%–12% Bis-Tris gels (NuPAGE, Invitrogen) and run for 1 h at 150 V. Proteins were transferred to PVDF membranes for 3 h on ice. After blocking in blocking buffer (LI-COR) and TBS-T for 1 h, membranes were incubated overnight with anti-RyR1 (1:5,000, mouse, ab2868, Abcam) and anti-12-kDa FK506 binding protein (FKBP12; 1:1,000 rabbit, ab2918, Abcam) antibodies. After washing with TBS-T, membranes were incubated in secondary antibody (1:20,000, IRDye 680-conjugated donkey anti-mouse IgG) and IRDye 800-conjugated donkey anti-rabbit IgG (926–68,072, 926–32,213, LI-COR Biosciences) for 1 h at room temperature. Membranes were washed three times with TBS-T and bands were visualized using an infrared fluorescence scanner (IR-Odyssey, LI-COR Biosciences). Band densities were analyzed with Image Studio Lite v 5.2 software (LI-COR). Data are expressed as ratios of FKBP12/RyR1 relative to the group mean of the RR group, which was set to 1.0.

Human proteomics analysis

Protein extraction and solubilization

Vastus lateralis muscle biopsies were homogenized in 16 μg/mL PBS and briefly centrifuged. After discarding the supernatant, 200 μL lysis buffer (8M Urea, 1% SDS, 50 mM Tris [pH 8.5], Roche protease and phosphatase inhibitor) were added to the pellet and samples were vortexed and sonicated on ice. Cell lysates were then centrifuged for 10 min at 4°C and 15,000 rpm and cleared lysates were transferred to new tubes. The extracted proteins were precipitated with chilled acetone (1:4 vol) at −20°C overnight and then centrifuged for 20 min at 14,000 × *g* at 4°C. The protein pellets were dissolved in 40 μL of 8 M urea and a 3 μL aliquot of each sample was diluted 10-fold to BCA-assay. A volume equivalent of 25 μg of proteins from each sample were adjusted to 43 μL with water and 5 μL of 1 M ammonium bicarbonate (AmBic) was added.

In solution digestion and TMT-labeling

Proteins were reduced with adding 1.5 μL of 200 mM dithiothreitol (DTT, Sigma) in 500 mM AmBic and incubated at 37°C for 1 h with shaking at 400 rpm. Alkylation was performed with adding 1.5 μL of 66 mM iodoacetamide (Sigma) in 500 mM AmBic at room temperature for 30 min with shaking at 400 rpm. Thereafter 1 μg of sequencing grade modified Trypsin (Promega) was added to each sample (1:33 trypsin:protein) and incubated for 16 h at 37°C. The digestion was stopped by adding of formic acid at final concentration of 5% and incubating the solution for 20 min at 37°C. Then the samples were cleaned on a C18 Hypersep plate (Thermo Scientific), dried using a Speedvac and re-suspended in 70 μL of 50 mM triethylammonium bicarbonate (TEAB) buffer and 30 μL of TMT-10plex (Thermo Scientific) reagent was added in dry acetonitrile (ACN) following incubation for 2 h at room temperature with shaking at 550 rpm. Labeling reaction was quenched with 11 μL of 5% hydroxylamine. Labeled samples were combined and dried on Speedvac. Following a cleaning on StageTip C18, 20 μL of the combined samples were dissolved in 0.1% formic acid and 2% ACN.

PRLC-MS/MS analysis

Chromatographic separation of peptides was achieved using a 50 cm C18 Easy-C18 column (Thermo Scientific) connected to nanoLC-1000 system (Thermo Scientific). Approximately 1.3 μg peptides were loaded onto the column in a volume of 2 μL and then eluted at a 300 nL/min flow rate for 180 min at a linear gradient from 4% to 26% ACN in 0.1% formic acid. Orbitrap Q Exactive plus mass spectrometer (Thermo Scientific) analyzed the eluted peptides that were ionized with electrospray ionization. The survey MS spectrum was acquired at the resolution of 140,000 in the range of m/z 350–1600. MS/MS data were obtained with a higher-energy collisional dissociation (HCD) for ions with charge z = 2–3 at a resolution of 70,000 using m/z 2 isolation width.

Proteomics data analysis

Data were analyzed on Proteome Discoverer v2.2 (Thermo Scientific) identifying protein in SwissProt database and the extracted abundances were further evaluated using an in-house developed R algorithm calculating fold changes and p values. Data were visualized using Qlucore Omics Explorer (Lund, Sweden).

RNA sequencing in BAT of *Actn3* KO and WT mice

Brown adipose tissue (BAT) was collected from *Actn3* WT and KO mice after 5 h of core body temperature analyses across the three treatment groups (thermoneutral [TN], room-temperature [RT], and cold exposed [CE]). A total of 18 WT and 16 KO mice underwent RNA sequencing using the Illumina HiSeq 2500 platform as per manufacturer instructions. Raw read data was processed using the Illumina BaseSpace RNA Express application (Illumina). Briefly, sequencing reads were aligned using STAR ultrafast RNA seq aligner[25] in the SAM file format,[26] then counted using HTSeq.[27] The resulting genewise count data was analyzed using the R (3.6.0) statistical programming language (R Core Team). Modeling of differential expression was conducted using the voom precision weights approach[28] in the limma (3.40.6)[29] package from the Bioconductor (3.9) project.

Statistics

Statistical analyses were performed using GraphPad Prism 8. Unpaired t tests or one-way ANOVA with Tukey's post hoc test were used to assess statistical significance between groups. Two-way repeated-measures ANOVA with Tukey's post hoc test was used when two subsequent measurements were performed in the same individual. Mantel-COX log-rank test was used for comparisons of the effect of cold-water immersion (baseline to end-point). Data are presented as mean ± SEM and $p \geq 0.05$ was considered statistically significant.

Results

Cold-water exposure of XX and RR individuals

Young male XX and RR individuals (Table S1) were immersed in 14°C water for 20 min periods interposed by 10 min pauses in room-temperature air; cold-water exposure was continued until the rectal temperature reached 35.5°C or for a total of 120 min (170 min including the pauses). The percentage of individuals able to maintain their body temperature above 35.5°C for the complete cold-water exposure was markedly higher in the XX group (69%) than in the RR group (30%)

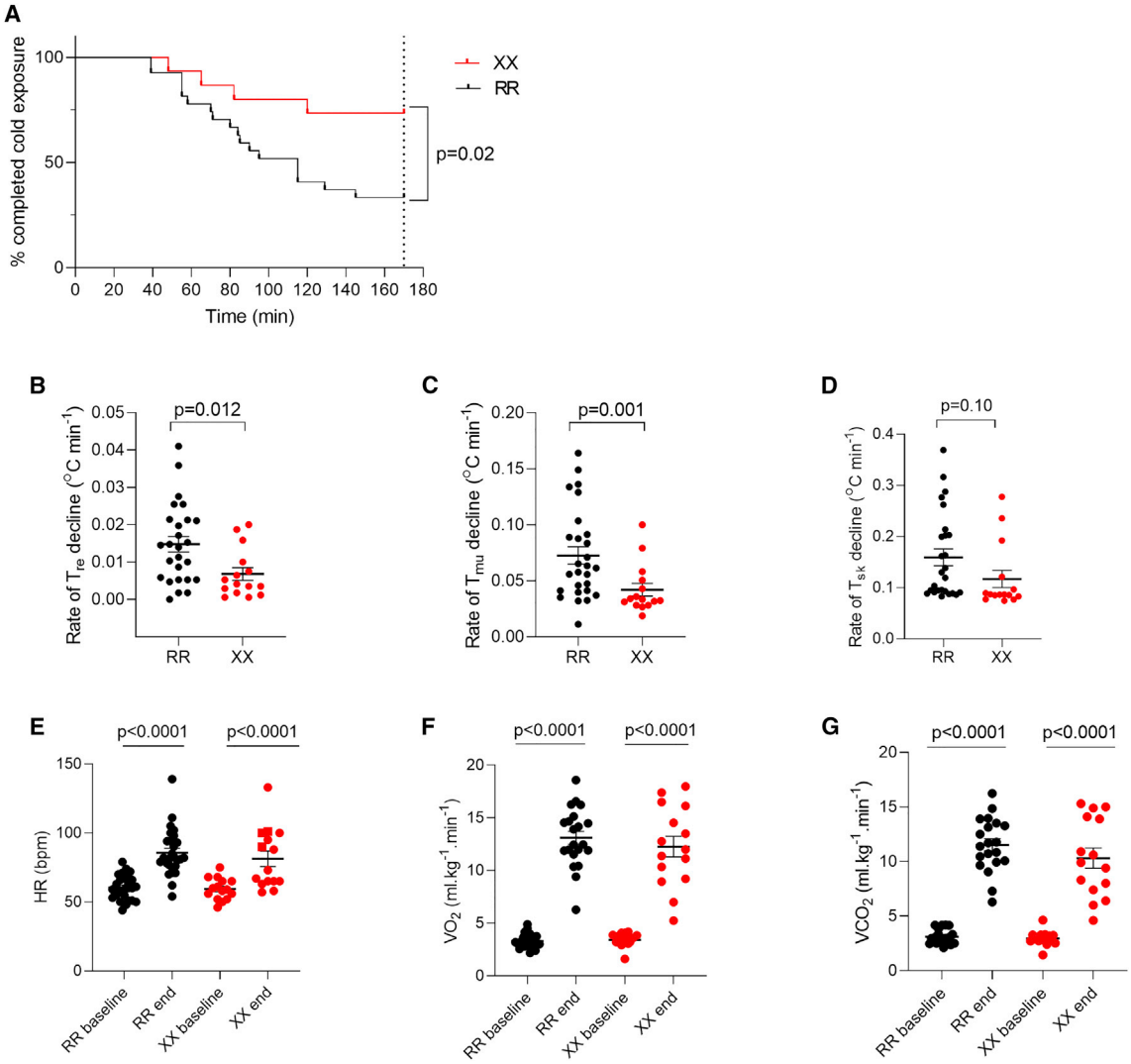

Figure 1. Temperature measurements and physiological responses during cold-water immersion

(A) Survival plot of the time taken to reach a rectal temperature (T_{re}) of 35.5°C or sustaining the complete 170 min period of cold-water immersion in RR (n = 27) and XX (n = 15) individuals. Log-rank (Mantel-COX) test was used to assess statistical difference between RR and XX individuals.

(B–D) The decline rate in rectal (T_{re}), intramuscular (T_{mu}), and skin (T_{sk}) temperatures in RR and XX subjects. Statistical difference between the two groups was assessed with unpaired t test.

(E–G) Heart rate and rate of pulmonary O_2 uptake (VO_2) and CO_2 exhalation (VCO_2) before (baseline) and at the end of cold-water immersion in RR and XX subjects. Statistical assessment with 2-way RM ANOVA revealed no differences between the two groups either before or at the end of cold-water exposure. Plots show values for each RR (black circles) and XX (red circles) individual and mean ± SEM.

(Figure 1A). The average rate of decline of rectal (T_{re}) and gastrocnemius muscle (T_{mu}) temperatures in XX subjects was about half of that in RR subjects (Figures 1B and 1C). The rate of skin temperature (T_{sk}) decline, on the other hand, was not significantly different between the two groups (Figure 1D). The dates of experiments were relatively evenly distributed over the year except for fewer experiments during the summer months (June-September). There was no obvious difference in the rates of temperature decline depending on when during the year experiments were performed (Figure S1). Thus, no obvious cold adaption over the winter months was detected in the present experiments, which fits with the concept that factors such as clothing, houses, and behavioral changes are more important than physiological adaptations for coping with a cold climate in modern societies.[30]

The overall increase in energy consumption induced by the cold challenge was assessed by measurements of heart rate and the rate of respiratory O_2 uptake (VO_2) and CO_2 exhalation (VCO_2); all three rates were significantly increased at the end of cold exposure irrespective of ACTN3 genotype (Figures 1E–1G). Thus, α-actinin-3-deficient individuals showed superior protection of core body temperature during an acute cold stress and this was achieved without increased energy consumption as judged from similar cold-induced increases in heart rate, VO_2, and VCO_2 in XX and RR individuals.

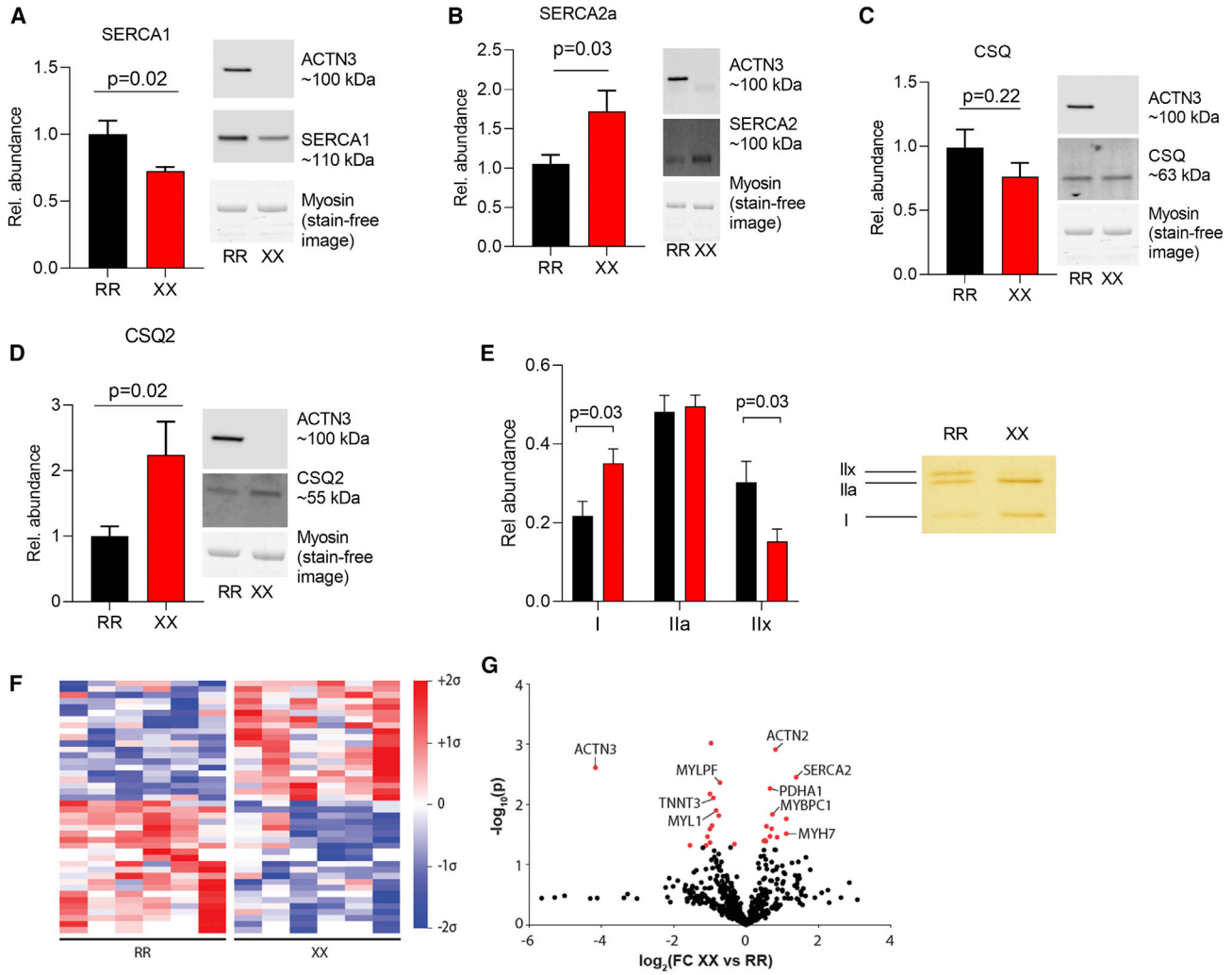

Figure 2. ACTN3 deficiency is accompanied by a shift toward a slower skeletal muscle phenotype

(A–D) Summary data (mean ± SEM) and representative western blots of the SR Ca^{2+}-handling proteins SERCA1, SERCA2a, CSQ, and CSQ2 in muscle of RR (n = 8) and XX (n = 7) individuals. Band intensities were normalized to their respective myosin loading controls. Data expressed relative to the mean value of the RR group, which was set to 1.0. Statistical difference between the two groups was assessed with unpaired t test.

(E) Silver-stained gels were used to assess the distribution of MyHC isoforms in RR (n = 7) and XX (n = 7) individuals. Right part shows a representative example of the distribution of MyHC in RR and XX individuals. The total staining of the three MyHC bands was set to 1 in each subject. Statistical difference between the two groups was tested with unpaired t test.

(F) Mean-centered sigma-normalized heatmap of differentially expressed proteins ($p < 0.05$).

(G) Volcano plot of all identified proteins (n = 601) expressed as fold-change (FC) in XX compared to RR individuals. Differentially abundant proteins are indicated in red.

Muscle protein analyses in XX and RR individuals

In mice, *Actn3* knockout (KO) results in changes in intracellular Ca^{2+} handling with marked increases in SR Ca^{2+} leak and the subsequent heat-generating active sarcoplasmic reticulum (SR) Ca^{2+} re-uptake via SERCA.[31] Uncoupling of SERCA activity from the actual Ca^{2+} transport into the SR is considered a key component in muscular non-shivering thermogenesis.[32–35] SERCA is expressed in several different isoforms in mammalian tissues, with SERCA1 and SERCA2a being the main isoforms in adult fast-twitch and slow-twitch muscle fibers, respectively.[36–38] Notably, we detected a shift in dominance from SERCA1 in RR muscles to SERCA2a in XX muscles (Figures 2A and 2B). The SR Ca^{2+} storage protein CSQ also shows a fiber type-dependent isoform distribution with CSQ1 dominating in fast-twitch fibers and CSQ2 in slow-twitch fibers.[37,39] We observed similar total CSQ expression in XX and RR muscles, whereas the expression of CSQ2 was about twice as high in XX compared to RR muscles (Figures 2C and 2D). The difference in SERCA and CSQ isoform expression between XX and RR muscles may reflect a larger volume of the muscle to be composed of slow-twitch fibers in XX than in RR subjects. Therefore, we used high-sensitivity silver staining to analyze the MyHC composition and found that XX muscles had significantly more slow-type MyHC I (β-MyHC) and less fast-type MyHC IIx than RR muscles (Figure 2E).

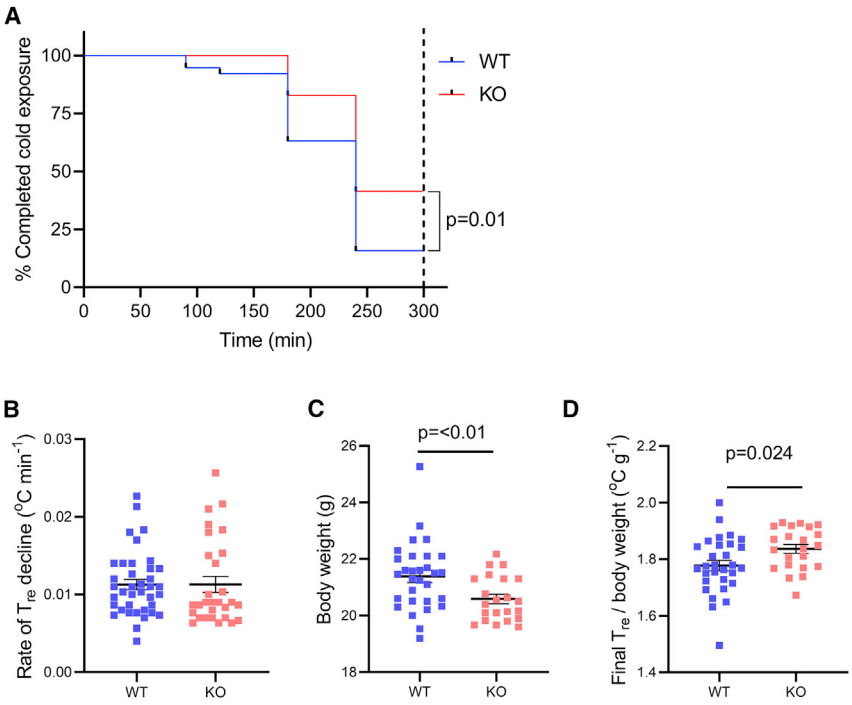

Figure 3. Improved cold tolerance in *Actn3* KO mice

(A) Survival plot of the time taken to reach 35.5°C core body temperature within 5 h exposure to 4°C air temperature in WT (n = 38, blue line) and *Actn3* KO (n = 29, red line) mice. Log-rank (Mantel-COX) test was used to assess statistical difference between WT and KO mice.

(B and C) The rate of decline in rectal temperature and body weight of WT and *Actn3* KO mice.

(D) The rectal temperature at the end of the 5 h of cold exposure plotted against the body weight.

Plots in (B)–(D) show values for each WT (blue squares) and *Actn3* KO (red squares) mouse and mean ± SEM. Statistical differences between the two groups assessed with unpaired t test.

The sarcomeric α-actinins are known to interact with a multitude of functionally diverse proteins involved in structural, metabolic, signaling, and Ca^{2+}-handling pathways.[7] We used proteomics as an exploratory measure to look for further differences in muscle between XX and RR individuals. This proteomic analysis of skeletal muscle biopsies shows distinct differences in protein abundance between XX and RR individuals. Overall, we found 42 proteins to be differentially expressed between genotypes (Figure 2F), including higher protein levels of slow-twitch muscle fiber markers (MyHC I [MYH7], slow-type myosin-binding protein C [MYBPC1], SERCA2) and lower levels of fast-twitch markers (myosin light chain 1/3 [MYL1], myosin regulatory light chain 2 [MYLPF], fast-type muscle troponin T [TNNT3]) in XX than in RR individuals (Figure 2G). Furthermore, pathway analysis revealed that differentially expressed proteins were enriched in pyruvate metabolism (p = 0.0003; FDR = 0.02), including pyruvate dehydrogenase (PDHA1) with an ~60% higher protein expression in XX than in RR individuals.

Although the difference in SERCA and CSQ isoform expression between XX and RR muscle homogenates corresponds with the MyHC distributions, α-actinin-3 deficiency might still affect the abundance of these Ca^{2+}-handling proteins within individual fiber types. However, fiber type-specific western blots performed on pooled single muscle fibers did not reveal any fiber type-dependent differences in the expression of SERCA1, total CSQ or CSQ2 between XX and RR muscles (Figure S2). Intriguingly, SERCA2a was higher in the RR than in XX type I fibers, which might indicate that the abundance of SERCAs is not the limiting factor in temperature regulation. SERCA might be involved in muscular non-shivering thermogenesis via its associated protein SLN, which interferes with SERCA function by mediating uncoupling of the SR Ca^{2+} uptake from the heat-generating ATP hydrolysis.[33,40] Hence, we measured SLN expression in muscle homogenates and in pooled single fibers, and the results showed no difference in SLN expression between XX and RR muscles (Figure S3 and S4). Another potential Ca^{2+}-SR-related mechanism for heat generation is Ca^{2+} leak through the SR Ca^{2+} release channel, the RyR1 channel complex, due to dissociation of the channel-stabilizing subunit FKBP12.[41,42] However, immunoprecipitation experiments did not reveal any difference in the amount of FKBP12 bound to RyR1 between XX and RR muscles (Figure S3B). To summarize, we could not detect any SR Ca^{2+}-handling protein-dependent explanation for the superior cold tolerance of XX subjects.

Cold exposure and brown adipose tissue analyses in *Actn3* KO mice

Brown adipose tissue (BAT) has been shown to function as a heat-generating organ especially in hibernating mammals and human infants.[43] Adult humans have little BAT (<5% of total fat mass[44]) and it is difficult to assess its importance as a heat generator.[45,46] We therefore utilized the well-defined *Actn3* KO mouse model to examine the impact of BAT activation as a mechanism for improved heat generation in α-actinin-3-deficient individuals.[4] Adult wild-type (WT) and *Actn3* KO mice were kept in a cold (4°C) room for 5 h and core body temperature was measured at regular intervals using a rectal probe. In accordance with the human results, the number of mice able to maintain their body temperature above 35.5°C for the cold exposure period was markedly higher in the *Actn3* KO (41%) than in the WT (16%) group (Figure 3A). Although the overall rate of temperature decline during cold exposure was not significantly

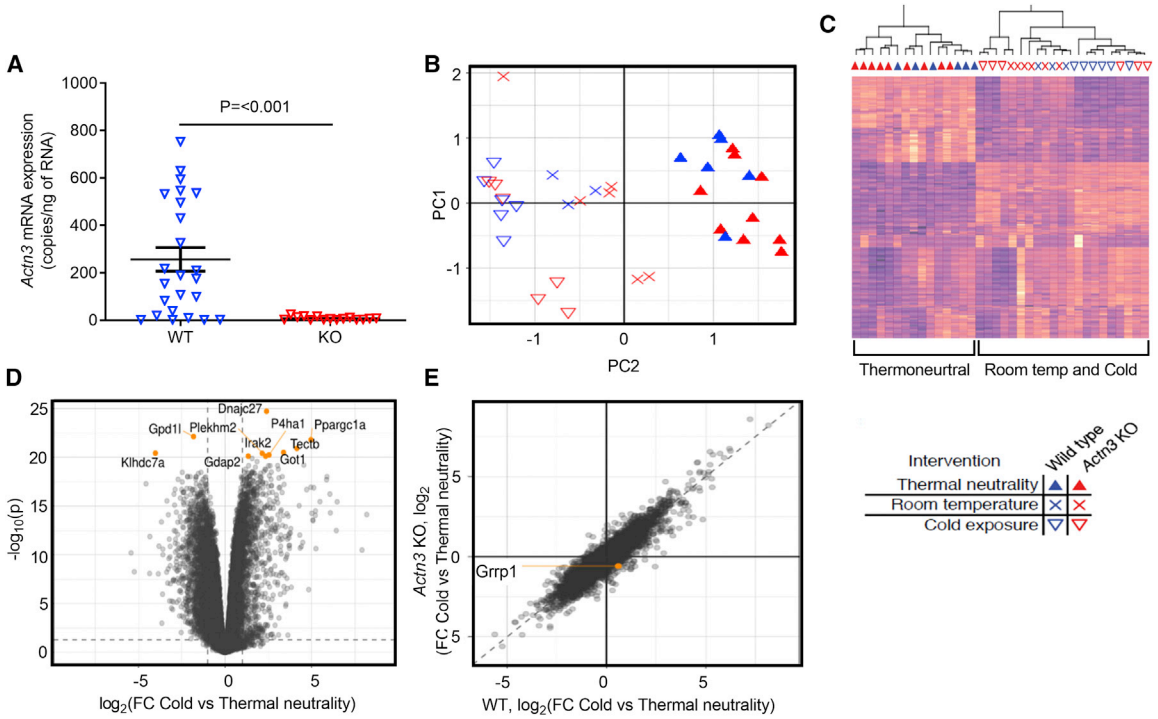

Figure 4. Acute cold exposure induced major, but *Actn3* genotype-independent, changes in mouse BAT gene expression
(A) Following cold exposure, *Actn3* mRNA is present in WT but not in *Actn3* KO mice. Plot show values for each WT (blue triangles) and *Actn3* KO (red triangles) mouse and mean ± SEM. Statistical difference between the two groups assessed with unpaired t test.
(B and C) RNA-sequencing analyses show an effect of temperature but no effect of *Actn3* genotype on BAT gene expression with both the principal component analysis (PCA) and heatmap. Description of symbols below heatmap refers to both PCA (B) and heatmap (C).
(D) Volcano plot of altered genes confirms that marked changes in BAT gene expression occurs following acute cold exposure, with >2,000 differentially expressed genes identified. Genes showing the largest changes are specified in Table S2.
(E) Interaction plot shows no general difference based on *Actn3* genotype in BAT following acute cold exposure.

different between the two groups (Figure 3B), *Actn3* KO mice were significantly lighter than their WT counterparts (Figure 3C) and therefore showed an improved cold tolerance after normalizing for body weight (Figure 3D).

Following cold exposure, *Actn3* mRNA was present in BAT of WT mice, but absent in the KO mice (Figure 4A). RNA sequencing was performed on BAT collected from mice subjected to either thermal neutrality (TN, 30°C), room temperature (RT, 22°C), or low temperature (cold, 4°C). An unbiased principal component analysis (PCA) and heatmap clustering separated samples based on temperature (TN, RT, and cold), whereas no consistent effect of *Actn3* genotype was observed (Figures 4B and 4C). Further analysis showed more than 2,000 differentially expressed genes in BAT following cold exposure (Figure 4D). However, an interaction plot shows no general difference based on *Actn3* genotype in BAT after acute cold exposure with only one transcript being significantly altered based on genotype and temperature (cold; glycine/arginine rich protein 1 [*Grrp1*], thus excluding any physiologically relevant genotype-specific difference in BAT properties after acute cold exposure (Figure 4E).

Muscle activation during cold-water exposure in XX and RR individuals

The major heat-generating mechanism in mammalian skeletal muscle during an acute cold challenge is involuntary activation of motor units resulting in skeletal muscle contraction. This mechanism is generally referred to as shivering thermogenesis although it involves both increased basal muscle tone due to continuous low-intensity activation and overt shivering due to high-intensity bursting activity.[47] In our human cohort, we used surface electromyography (EMG) to follow the activation of pectoralis major muscles during cold-water immersion and observed more frequent bursting activity in RR individuals with mean data showing an approximately two times higher rate of bursts in RR than in XX muscles (Figures 5A and 5B); the markedly higher activity during bursts also resulted in a slightly higher mean EMG signal frequency in RR muscles (Figure 5C). On the other hand, there was no significant difference in the amplitude of the EMG signal, which reflects the overall number of muscle fibers being activated (Figure 5D).

Discussion

We here show an improved body temperature defense during cold-water immersion in humans deficient of the sarcomeric protein α-actinin-3 expressed in fast-twitch skeletal muscle. Intriguingly, the improved cold tolerance in XX individuals was not accompanied by increased energy consumption as judged from similar cold challenge-induced increases in heart rate, VO_2, and VCO_2 in XX

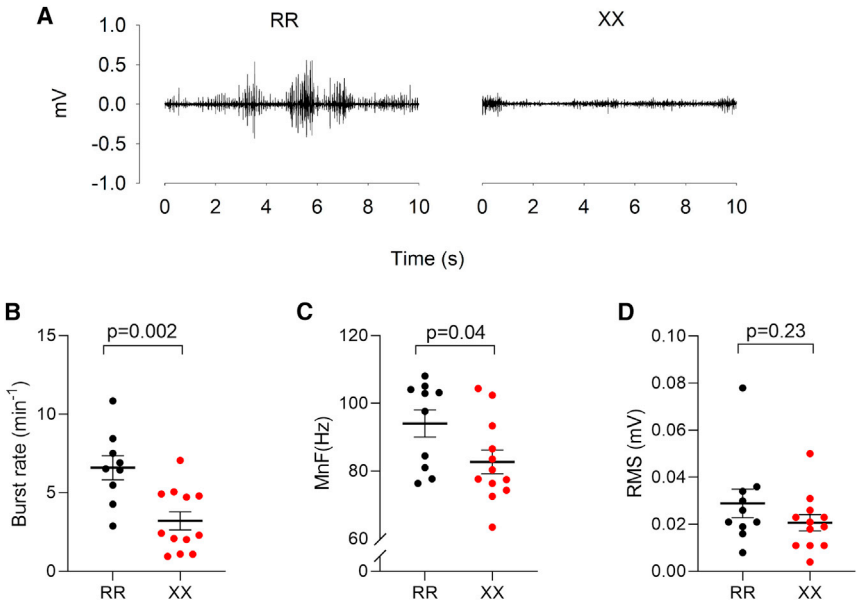

Figure 5. Bursting muscle activity rather than increased muscle tone is more prominent in RR muscles

(A) Representative EMG records from pectoralis major muscles during cold exposure showing continuous low-intensity activity in the XX individual and frequent bursts of high-intensity activity in the RR individual.

(B–D) Summary data of the burst rate, mean EMG signal frequency (MnF), and amplitude (RMS, root mean square). Plots show values for each RR (black circles) and XX (red circles) individual and mean ± SEM. Statistical differences between RR and XX individuals were assessed with unpaired t test.

and RR individuals. Our results thus provide a physiological mechanism underlying this energy-efficient cold protection in XX individuals: more slow-type I MyHC in XX muscle coupled to a shift in neuronal muscle activation toward increased muscle tone rather than overt shivering.

Previous studies have not shown any, or only minor, shifts toward more slow-twitch type I fibers and less fast-twitch type II fibers in XX than in RR muscle.[48–50] On the other hand, the cross-sectional area of type II fibers might be larger in RR than in XX individuals.[49,51] Moreover, the absence of the structural protein α-actinin-3 limits the response in type II fibers to strength- and power-oriented training and XX individuals are underrepresented in elite power/sprint athletes.[6,8,52] Thus, rather than a difference in the number of type I versus type II fibers, the shift toward more type I MyHC in the present XX individuals is likely due to a smaller cross-sectional area of type II fibers (and/or larger area of type I fibers) in XX than in RR muscle.

Cold-induced low-intensity continuous muscle activity, i.e., increased muscle tone, is associated with activation of type I muscle fibers, whereas high-intensity burst activity is linked to the recruitment of type II muscle fibers.[53–55] Thus, our finding of a higher burst rate in RR than in XX muscles is consistent with the larger proportion of type II MyHC in RR muscles. Importantly, given that the superior cold resistance in XX individuals was not accompanied by any signs indicating a larger increase in energy consumption, low-intensity tonic activation of type I muscle fibers appears as an energetically effective way to generate heat.[54] In conjunction with the increased frequency of the X-allele in colder climates, this finding indicates an evolutionary survival advantage of α-actinin-3 deficiency as humans migrated to colder climates.

Infant survival would have been an important factor during the human migration to colder climates. While our data demonstrate an important role of ACTN3 in adults, it remains to be determined whether α-actinin-3 deficiency affects the cold tolerance of human infants. First, it is uncertain whether the shift toward more type I MyHC in XX individuals is present already at birth, hence contributing to the protection against infant mortality when moving to a colder environment, or whether it develops later in life as an adaptive response to strength-related physical activities. Second, BAT constitutes a significant heat source in human infants.[43,46] We here show expression of *Actn3* in BAT of adult mice following acute cold exposure. Although we could not detect any physiologically relevant *Actn3* genotype-specific difference in BAT properties after acute cold exposure, our data do not exclude the possibility of an α-actinin-3-dependent effect on BAT thermogenesis in human infants.

In conclusion, α-actinin-3-deficient humans exhibit improved cold tolerance during cold-water immersion linked to a shift toward more slow-twitch type I MyHC and an energetically effective heat-generating increase in muscle tone rather than overt shivering. These findings provide a mechanism for the increase in X-allele frequency as modern humans migrated from Africa to the colder climates of central and northern Europe over 50,000 years ago.[9,10]

Data and code availability

The mass spectrometry proteomics data have been deposited to the ProteomeXchange Consortium via the PRIDE[56] partner repository with the dataset identifier PXD022997.

The RNA sequencing in mouse BAT data have been deposited in NCBI's Gene Expression Omnibus and are accessible through GEO: GSE164936 (https://www.ncbi.nlm.nih.gov/geo/query/acc.cgi?acc=GSE164936).

Supplemental information

Supplemental information can be found online at https://doi.org/10.1016/j.ajhg.2021.01.013.

Acknowledgments

This study was funded by grants to H.W. from the Swedish Medical Research Council (2018-02576) and the Swedish Research Council for Sport Science (P2019-060); to M.B. from the Research Council of Lithuania (S-02/SMT12P-014 and 01/SMT13P-176); to D.C.A. from the Swedish Society for Medical Research (SSMF, S16-0159), the Jeansson's Foundation (JS2018-0131), and the Swedish Heart-Lung Foundation (20180637, 2016074); and to K.N.N. from the Australian National Health and Medical Research Council (NHMRC, APP1130215). We thank Monika Kisieliute and Andreius Subocius for their assistance in genotyping and collection of human muscle biopsies. We also thank Sophie Agius and Alison Burns for their contribution to maintaining the *Actn3* KO mouse colony.

Declaration of interests

V.M.L. is founder, CEO, and shareholder of HepaPredict AB. In addition, V.M.L. discloses consultancy work for EnginZyme AB.

Received: October 28, 2020
Accepted: January 19, 2021
Published: February 17, 2021

Web Resources

GEO, https://www.ncbi.nlm.nih.gov/geo/
NCBI Resources Gene, https://www.ncbi.nlm.nih.gov/gene
OMIM, https://www.omim.org/
Pride, http://www.ebi.ac.uk/pride

References

1. Mills, M., Yang, N., Weinberger, R., Vander Woude, D.L., Beggs, A.H., Easteal, S., and North, K. (2001). Differential expression of the actin-binding proteins, alpha-actinin-2 and -3, in different species: implications for the evolution of functional redundancy. Hum. Mol. Genet. *10*, 1335–1346.
2. North, K.N., Yang, N., Wattanasirichaigoon, D., Mills, M., Easteal, S., and Beggs, A.H. (1999). A common nonsense mutation results in alpha-actinin-3 deficiency in the general population. Nat. Genet. *21*, 353–354.
3. Quinlan, K.G., Seto, J.T., Turner, N., Vandebrouck, A., Floetenmeyer, M., Macarthur, D.G., Raftery, J.M., Lek, M., Yang, N., Parton, R.G., et al. (2010). Alpha-actinin-3 deficiency results in reduced glycogen phosphorylase activity and altered calcium handling in skeletal muscle. Hum. Mol. Genet. *19*, 1335–1346.
4. MacArthur, D.G., Seto, J.T., Raftery, J.M., Quinlan, K.G., Huttley, G.A., Hook, J.W., Lemckert, F.A., Kee, A.J., Edwards, M.R., Berman, Y., et al. (2007). Loss of *ACTN3* gene function alters mouse muscle metabolism and shows evidence of positive selection in humans. Nat. Genet. *39*, 1261–1265.
5. Houweling, P.J., Papadimitriou, I.D., Seto, J.T., Pérez, L.M., Coso, J.D., North, K.N., Lucia, A., and Eynon, N. (2018). Is evolutionary loss our gain? The role of ACTN3 p.Arg577Ter (R577X) genotype in athletic performance, ageing, and disease. Hum. Mutat. *39*, 1774–1787.
6. Pickering, C., and Kiely, J. (2018). *ACTN3*, morbidity, and healthy aging. Front. Genet. *9*, 15.
7. Lee, F.X., Houweling, P.J., North, K.N., and Quinlan, K.G. (2016). How does α-actinin-3 deficiency alter muscle function? Mechanistic insights into ACTN3, the 'gene for speed'. Biochim. Biophys. Acta *1863*, 686–693.
8. Del Coso, J., Hiam, D., Houweling, P., Pérez, L.M., Eynon, N., and Lucía, A. (2019). More than a 'speed gene': ACTN3 R577X genotype, trainability, muscle damage, and the risk for injuries. Eur. J. Appl. Physiol. *119*, 49–60.
9. Friedlander, S.M., Herrmann, A.L., Lowry, D.P., Mepham, E.R., Lek, M., North, K.N., and Organ, C.L. (2013). ACTN3 allele frequency in humans covaries with global latitudinal gradient. PLoS ONE *8*, e52282.
10. Amorim, C.E.G., Acuña-Alonzo, V., Salzano, F.M., Bortolini, M.C., and Hünemeier, T. (2015). Differing evolutionary histories of the ACTN3*R577X polymorphism among the major human geographic groups. PLoS ONE *10*, e0115449.
11. Tikuisis, P., Jacobs, I., Moroz, D., Vallerand, A.L., and Martineau, L. (2000). Comparison of thermoregulatory responses between men and women immersed in cold water. J Appl Physiol (1985) *89*, 1403–1411.
12. McArdle, W.D., Magel, J.R., Gergley, T.J., Spina, R.J., and Toner, M.M. (1984). Thermal adjustment to cold-water exposure in resting men and women. J. Appl. Physiol. *56*, 1565–1571.
13. Houweling, P.J., Berman, Y.D., Turner, N., Quinlan, K.G.R., Seto, J.T., Yang, N., Lek, M., Macarthur, D.G., Cooney, G., and North, K.N. (2017). Exploring the relationship between α-actinin-3 deficiency and obesity in mice and humans. Int. J. Obes. *41*, 1154–1157.
14. Venckunas, T., Skurvydas, A., Brazaitis, M., Kamandulis, S., Snieckus, A., and Moran, C.N. (2012). Human alpha-actinin-3 genotype association with exercise-induced muscle damage and the repeated-bout effect. Appl. Physiol. Nutr. Metab. *37*, 1038–1046.
15. Brazaitis, M., Eimantas, N., Daniuseviciute, L., Mickeviciene, D., Steponaviciute, R., and Skurvydas, A. (2014). Two strategies for response to 14 °C cold-water immersion: is there a difference in the response of motor, cognitive, immune and stress markers? PLoS ONE *9*, e109020.
16. Brazaitis, M., Paulauskas, H., Skurvydas, A., Budde, H., Daniuseviciute, L., and Eimantas, N. (2016). Brief rewarming blunts hypothermia-induced alterations in sensation, motor drive and cognition. Front. Physiol. *7*, 592.
17. Solianik, R., Skurvydas, A., Mickevičienė, D., and Brazaitis, M. (2014). Intermittent whole-body cold immersion induces similar thermal stress but different motor and cognitive responses between males and females. Cryobiology *69*, 323–332.
18. Knights, A.J., Vohralik, E.J., Houweling, P.J., Stout, E.S., Norton, L.J., Alexopoulos, S.J., Yik, J.J., Mat Jusoh, H., Olzomer, E.M., Bell-Anderson, K.S., et al. (2020). Eosinophil function in adipose tissue is regulated by Krüppel-like factor 3 (KLF3). Nat. Commun. *11*, 2922.
19. Lenhardt, R., and Sessler, D.I. (2006). Estimation of mean body temperature from mean skin and core temperature. Anesthesiology *105*, 1117–1121.
20. van Ooijen, A.M., van Marken Lichtenbelt, W.D., van Steenhoven, A.A., and Westerterp, K.R. (2005). Cold-induced heat production preceding shivering. Br. J. Nutr. *93*, 387–391.
21. Blondin, D.P., Labbé, S.M., Phoenix, S., Guérin, B., Turcotte, E.E., Richard, D., Carpentier, A.C., and Haman, F. (2015). Contributions of white and brown adipose tissues and skeletal muscles to acute cold-induced metabolic responses in healthy men. J. Physiol. *593*, 701–714.

22. Christiansen, D., MacInnis, M.J., Zacharewicz, E., Xu, H., Frankish, B.P., and Murphy, R.M. (2019). A fast, reliable and sample-sparing method to identify fibre types of single muscle fibres. Sci. Rep. *9*, 6473.
23. Lamboley, C.R., Wyckelsma, V.L., McKenna, M.J., Murphy, R.M., and Lamb, G.D. (2016). Ca^{2+} leakage out of the sarcoplasmic reticulum is increased in type I skeletal muscle fibres in aged humans. J. Physiol. *594*, 469–481.
24. Mizunoya, W., Wakamatsu, J., Tatsumi, R., and Ikeuchi, Y. (2008). Protocol for high-resolution separation of rodent myosin heavy chain isoforms in a mini-gel electrophoresis system. Anal. Biochem. *377*, 111–113.
25. Dobin, A., Davis, C.A., Schlesinger, F., Drenkow, J., Zaleski, C., Jha, S., Batut, P., Chaisson, M., and Gingeras, T.R. (2013). STAR: ultrafast universal RNA-seq aligner. Bioinformatics *29*, 15–21.
26. Li, H., Handsaker, B., Wysoker, A., Fennell, T., Ruan, J., Homer, N., Marth, G., Abecasis, G., Durbin, R.; and 1000 Genome Project Data Processing Subgroup (2009). The Sequence Alignment/Map format and SAMtools. Bioinformatics *25*, 2078–2079.
27. Anders, S., Pyl, P.T., and Huber, W. (2015). HTSeq–a Python framework to work with high-throughput sequencing data. Bioinformatics *31*, 166–169.
28. Law, C.W., Chen, Y., Shi, W., and Smyth, G.K. (2014). voom: Precision weights unlock linear model analysis tools for RNA-seq read counts. Genome Biol. *15*, R29.
29. Ritchie, M.E., Phipson, B., Wu, D., Hu, Y., Law, C.W., Shi, W., and Smyth, G.K. (2015). limma powers differential expression analyses for RNA-sequencing and microarray studies. Nucleic Acids Res. *43*, e47, e47.
30. Daanen, H.A., and Van Marken Lichtenbelt, W.D. (2016). Human whole body cold adaptation. Temperature (Austin) *3*, 104–118.
31. Head, S.I., Chan, S., Houweling, P.J., Quinlan, K.G., Murphy, R., Wagner, S., et al. (2015). Altered Ca^{2+} kinetics associated with α-actinin-3 deficiency may explain positive selection for ACTN3 null allele in human evolution. PLoS Genet. *11*, e1004862.
32. de Meis, L. (2001). Role of the sarcoplasmic reticulum Ca^{2+}-ATPase on heat production and thermogenesis. Biosci. Rep. *21*, 113–137.
33. Bal, N.C., Maurya, S.K., Singh, S., Wehrens, X.H., and Periasamy, M. (2016). Increased reliance on muscle-based thermogenesis upon acute minimization of brown adipose tissue function. J. Biol. Chem. *291*, 17247–17257.
34. Nowack, J., Giroud, S., Arnold, W., and Ruf, T. (2017). Muscle non-shivering thermogenesis and its role in the evolution of endothermy. Front. Physiol. *8*, 889.
35. Rowland, L.A., Bal, N.C., and Periasamy, M. (2015). The role of skeletal-muscle-based thermogenic mechanisms in vertebrate endothermy. Biol. Rev. Camb. Philos. Soc. *90*, 1279–1297.
36. Periasamy, M., and Kalyanasundaram, A. (2007). SERCA pump isoforms: their role in calcium transport and disease. Muscle Nerve *35*, 430–442.
37. Schiaffino, S., and Reggiani, C. (2011). Fiber types in mammalian skeletal muscles. Physiol. Rev. *91*, 1447–1531.
38. Lamboley, C.R., Murphy, R.M., McKenna, M.J., and Lamb, G.D. (2014). Sarcoplasmic reticulum Ca^{2+} uptake and leak properties, and SERCA isoform expression, in type I and type II fibres of human skeletal muscle. J. Physiol. *592*, 1381–1395.
39. Lamboley, C.R., Murphy, R.M., McKenna, M.J., and Lamb, G.D. (2013). Endogenous and maximal sarcoplasmic reticulum calcium content and calsequestrin expression in type I and type II human skeletal muscle fibres. J. Physiol. *591*, 6053–6068.
40. Mall, S., Broadbridge, R., Harrison, S.L., Gore, M.G., Lee, A.G., and East, J.M. (2006). The presence of sarcolipin results in increased heat production by Ca^{2+}-ATPase. J. Biol. Chem. *281*, 36597–36602.
41. Aydin, J., Shabalina, I.G., Place, N., Reiken, S., Zhang, S.J., Bellinger, A.M., Nedergaard, J., Cannon, B., Marks, A.R., Bruton, J.D., and Westerblad, H. (2008). Nonshivering thermogenesis protects against defective calcium handling in muscle. FASEB J. *22*, 3919–3924.
42. Zalk, R., Clarke, O.B., des Georges, A., Grassucci, R.A., Reiken, S., Mancia, F., Hendrickson, W.A., Frank, J., and Marks, A.R. (2015). Structure of a mammalian ryanodine receptor. Nature *517*, 44–49.
43. Nedergaard, J., and Cannon, B. (2018). Brown adipose tissue as a heat-producing thermoeffector. Handb. Clin. Neurol. *156*, 137–152.
44. Leitner, B.P., Huang, S., Brychta, R.J., Duckworth, C.J., Baskin, A.S., McGehee, S., Tal, I., Dieckmann, W., Gupta, G., Kolodny, G.M., et al. (2017). Mapping of human brown adipose tissue in lean and obese young men. Proc. Natl. Acad. Sci. USA *114*, 8649–8654.
45. Ong, F.J., Ahmed, B.A., Oreskovich, S.M., Blondin, D.P., Haq, T., Konyer, N.B., Noseworthy, M.D., Haman, F., Carpentier, A.C., Morrison, K.M., and Steinberg, G.R. (2018). Recent advances in the detection of brown adipose tissue in adult humans: a review. Clin. Sci. (Lond.) *132*, 1039–1054.
46. Richard, M.A., Pallubinsky, H., and Blondin, D.P. (2020). Functional characterization of human brown adipose tissue metabolism. Biochem. J. *477*, 1261–1286.
47. Haman, F., and Blondin, D.P. (2017). Shivering thermogenesis in humans: Origin, contribution and metabolic requirement. Temperature (Austin) *4*, 217–226.
48. Norman, B., Esbjörnsson, M., Rundqvist, H., Österlund, T., Glenmark, B., and Jansson, E. (2014). *ACTN3* genotype and modulation of skeletal muscle response to exercise in human subjects. J Appl Physiol (1985) *116*, 1197–1203.
49. Vincent, B., De Bock, K., Ramaekers, M., Van den Eede, E., Van Leemputte, M., Hespel, P., and Thomis, M.A. (2007). ACTN3 (R577X) genotype is associated with fiber type distribution. Physiol. Genomics *32*, 58–63.
50. Ahmetov, I.I., Druzhevskaya, A.M., Lyubaeva, E.V., Popov, D.V., Vinogradova, O.L., and Williams, A.G. (2011). The dependence of preferred competitive racing distance on muscle fibre type composition and *ACTN3* genotype in speed skaters. Exp. Physiol. *96*, 1302–1310.
51. Broos, S., Malisoux, L., Theisen, D., van Thienen, R., Ramaekers, M., Jamart, C., Deldicque, L., Thomis, M.A., and Francaux, M. (2016). Evidence for *ACTN3* as a speed gene in isolated human mscle fibers. PLoS ONE *11*, e0150594.
52. Yang, N., MacArthur, D.G., Gulbin, J.P., Hahn, A.G., Beggs, A.H., Easteal, S., and North, K. (2003). *ACTN3* genotype is associated with human elite athletic performance. Am. J. Hum. Genet. *73*, 627–631.
53. Meigal, A. (2002). Gross and fine neuromuscular performance at cold shivering. Int. J. Circumpolar Health *61*, 163–172.
54. Lømo, T., Eken, T., Bekkestad Rein, E., and Nja, A. (2020). Body temperature control in rats by muscle tone during rest or sleep. Acta Physiol. (Oxf.) *228*, e13348.

55. Blondin, D.P., Frisch, F., Phoenix, S., Guérin, B., Turcotte, E.E., Haman, F., Richard, D., and Carpentier, A.C. (2017). Inhibition of intracellular triglyceride lipolysis suppresses cold-induced brown adipose tissue metabolism and increases shivering in humans. Cell Metab. *25*, 438–447.

56. Perez-Riverol, Y., Csordas, A., Bai, J., Bernal-Llinares, M., Hewapathirana, S., Kundu, D.J., Inuganti, A., Griss, J., Mayer, G., Eisenacher, M., et al. (2019). The PRIDE database and related tools and resources in 2019: improving support for quantification data. Nucleic Acids Res 47(D1):D442-D450 .